

ARTICLE

Received 17 Aug 2014 | Accepted 10 Apr 2015 | Published 20 May 2015

DOI: 10.1038/ncomms8183

Anomalous magnetoresistance in the spinel superconductor LiTi_2O_4

K. Jin^{1,2,3}, G. He¹, X. Zhang^{3,4}, S. Maruyama⁴, S. Yasui⁴, R. Suchoski⁴, J. Shin⁴, Y. Jiang³, H.S. Yu¹, J. Yuan¹, L. Shan^{1,2}, F.V. Kusmartsev⁵, R.L. Greene³ & I. Takeuchi⁴

LiTi_2O_4 is a unique compound in that it is the only known spinel oxide superconductor. The lack of high quality single crystals has thus far prevented systematic investigations of its transport properties. Here we report a careful study of transport and tunnelling spectroscopy in epitaxial LiTi_2O_4 thin films. An unusual magnetoresistance is observed which changes from nearly isotropic negative to prominently anisotropic positive as the temperature is decreased. We present evidence that shows that the negative magnetoresistance likely stems from the suppression of local spin fluctuations or spin-orbit scattering centres. The positive magnetoresistance suggests the presence of an orbital-related state, also supported by the fact that the superconducting energy gap decreases as a quadratic function of magnetic field. These observations indicate that the spin-orbital fluctuations play an important role in LiTi_2O_4 in a manner similar to high-temperature superconductors.

¹Beijing National Laboratory for Condensed Matter Physics, Institute of Physics, Chinese Academy of Sciences, Beijing 100190, China. ²Collaborative Innovation Center of Quantum Matter, Beijing 100190, China. ³Center for Nanophysics and Advanced Materials and Department of Physics, University of Maryland, College Park, Maryland 20742, USA. ⁴Department of Materials Science and Engineering, University of Maryland, College Park, Maryland 20742, USA. ⁵Department of Physics, Loughborough University, Loughborough LE11 3TU, UK. Correspondence and requests for materials should be addressed to K.J. (email: kuijin@iphy.ac.cn) or to R.L.G. (email: rgreene@squid.umd.edu) or to I.T. (email: takeuchi@umd.edu).

LiTi₂O₄ (LTO) is an oxide superconductor with a spinel crystal structure¹. It was discovered in early 1970's by Johnston *et al.*², and it has the superconducting transition temperature T_c of 11 K (ref. 1). Although its T_c can be described by band-structure calculations using the McMillan formula with a weak electron-phonon coupling constant ($\lambda_{\text{el-ph}} \sim 0.6$; refs 3,4), an enhanced density of states or an equivalently larger coupling constant has been unveiled from specific-heat^{5,6} and magnetic susceptibility measurements⁷. Other measurements like nuclear magnetic resonance⁸, point contact Andreev reflection spectroscopy⁹, and resonant inelastic soft-x-ray scattering¹⁰ have revealed the significance of d - d electron correlations. It is naturally expected that the correlations play a role in the microscopic mechanism for its superconductivity.

Moreover, in contrast to perovskite oxides, LTO has a cubic symmetry with the space group of $Fd\bar{3}m$, where the lithium and titanium cations are located at the tetrahedral $8a$ and octahedral $16d$ sites⁷, respectively. On one hand, the t_{2g} sub-band of Ti is in high degree of degeneracy, remaining in a narrow d -band metal with significant electron-electron interaction^{8,11}. On the other hand, the Ti sublattice, in mixed valences of Ti³⁺ and Ti⁴⁺, is frustrated and favours short-range spin ordering¹². Therefore, it is interesting to see whether spin-orbital fluctuations also play a role in superconductivity in LTO, akin to the perovskite-type high T_c superconductors^{13,14}. However, the development of an understanding of this system has been hampered by the lack of sample reproducibility and the availability of single crystals or high quality thin films^{1,7,15}. Recently, high quality epitaxial LTO thin films were successfully grown by pulsed laser deposition^{16,17}, thus opening the door for systematic experiments on LTO.

In this paper, we present results of transport and tunnelling studies on single crystalline-like epitaxial LTO thin films. The suppression of the superconducting energy gap as a quadratic

function of magnetic field, and an anomalous crossover of magnetoresistance from prominently anisotropic positive to nearly isotropic negative with increasing temperature have been observed for the first time. In addition to the extracted key parameters from the combined tunnelling and transport measurements, a full picture of LTO has emerged: the data suggest the presence of spin-orbit scattering/spin fluctuations below $\sim 100 \pm 10$ K and an orbital-related state below $T_{\text{ch}} \sim 50 \pm 10$ K. We propose a theoretical model to account for the relation between the superconducting energy gap and the magnetic field.

Results

Charge transport data and tunnelling spectra. The (00 $\bar{1}$)-oriented LTO thin films were epitaxially grown on (00 $\bar{1}$)-oriented MgAl₂O₄ substrates by pulsed laser deposition. Our LTO films consistently display T_c of 11 ± 0.25 K with narrow transition widths of < 0.5 K. We have found that different films have different residual resistivity ratios (RRR). The films were patterned into Hall bars to carry out Hall and normal resistivity measurements. Tunnelling spectroscopy was performed where Pt-Ir tips were used to make point contacts in the out-of-plane axis direction (c -axis, perpendicular to the film plane) of LTO¹⁸.

Figure 1a shows the resistivity versus temperature curves for samples with two different RRR ratios: 6.25 and 3 for samples L1 and L2, respectively. L1 and L2 have similar resistivity values at room temperature and the same T_c . The normal state resistivity of both samples can be fitted to a curve consistent with the Fermi liquid behaviour, $\rho = \rho_0 + AT^2$ (grey lines) from 40 to 120 K with residual resistivity (ρ_0) of $\approx 71 \mu\Omega \text{ cm}$ for L1 and $\approx 166 \mu\Omega \text{ cm}$ for L2. The deviation from the Fermi liquid behaviour at low temperatures is caused by an enhanced electron-electron

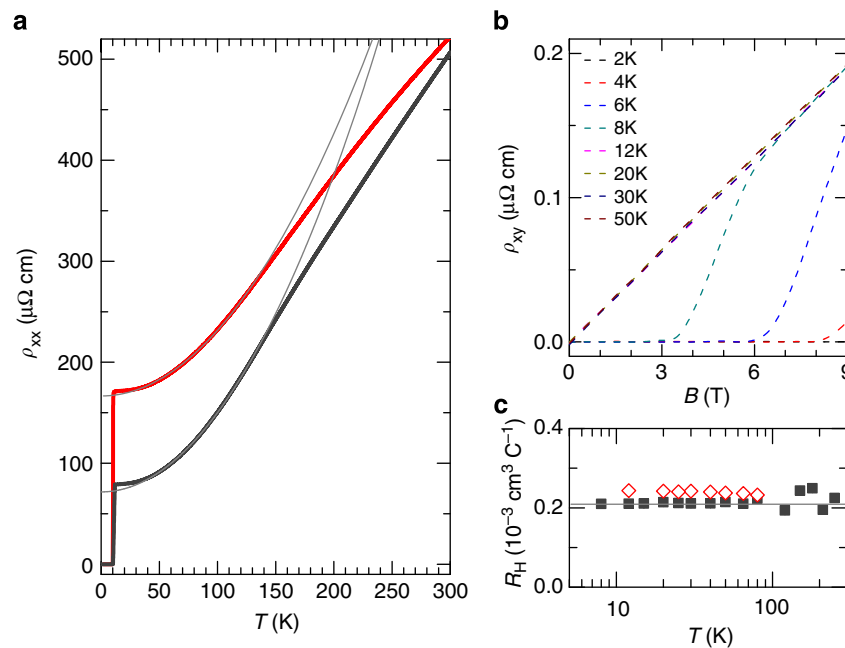


Figure 1 | Resistivity and Hall behavior of LiTi₂O₄ thin films. (a) $\rho_{xx}(T)$ of two samples. They have similar resistivity ($\sim 500 \mu\Omega \text{ cm}$) at room temperature, and the same T_c of 11 K, but different residual resistivity ratios (RRR): RRR ~ 6.25 for Sample L1 (black curve) and ~ 3 for the Sample L2 (red curve). The resistivity curve from 40 to 120 K can be fit by $\rho = \rho_0 + AT^2$ (grey lines). (b) The Hall resistivity is proportional to the magnetic field at different temperatures, and all the $\rho_{xy}(B)$ curves overlap in the normal state (only data on Sample L1 are shown here), suggesting a simple one band-structure and a temperature-independent Hall coefficient. Note that at very low temperatures, the magnetic field is not sufficient to suppress the superconductivity ($B \perp ab$ plane). (c) Hall coefficient versus temperature for both samples (L1: solid symbols. L2: open symbols). Though the two samples show different RRR, their Hall coefficient values are very close to each other. Assuming $R_H = 1/(ne)$, we find a hole concentration of $\sim 3 \times 10^{22} \text{ cm}^{-3}$, which is almost constant over the entire measured temperature range.

interaction as discussed below. By sweeping the magnetic field perpendicular to the film surface ($B \perp$ in-plane (ab plane)) at fixed temperatures, the Hall resistivity, that is, $\rho_{xy} = \frac{E_y}{j_x} = \frac{V_y t}{I_x}$, has been extracted. ρ_{xy} data for different temperatures are plotted in Fig. 1b, where V_y is the Hall voltage obtained by subtracting the transverse voltage in negative field from that in positive field, and t is the thickness of the film. In the normal state, the Hall resistivity is always proportional to the magnetic field, positive and temperature independent, strongly suggesting the presence of one type of charge carriers (holes) and a simple electronic band structure. The charge carrier concentration is calculated assuming a parabolic band structure, that is, the Hall coefficient $R_H = \frac{1}{ne}$. L1 and L2 have almost the same hole concentration of $\sim 3 \times 10^{22} \text{ cm}^{-3}$ (Fig. 1c), indicating that the different RRRs are likely caused by the difference in mobility values.

The point contact measurements were carried out on L1 before it was patterned into a Hall bar for transport measurements. As described by the Blonder, Tinkham and Klapwijk (BTK) model¹⁹, the tunnelling regime is achieved for $Z > 1$, where Z represents the tunnelling barrier height and the Fermi velocity mismatch²⁰. The differential conductance spectrum shows a clear temperature and field-dependent coherence peak. The normalized differential conductance spectra with and without applied magnetic field are shown in Fig. 2a–c as a function of bias voltage (see Supplementary Note 1 for normalization procedure). The normalized experimental curves were fitted using a modified BTK model with a complex energy $E' = E + i\Gamma$ (ref. 21). The broadening Γ term, which takes into account sample inhomogeneity and a finite quasi-particle lifetime by scattering, is temperature independent in zero field, but application of magnetic field has been found to lead to an additional pair-breaking factor²², which in effect is akin to an enhanced Γ (ref. 23).

Fitting parameters and superconducting energy gap. Several key points can be made from the fitting of our tunnelling spectra. First, the Z value of our Pt–Ir/LTO junction is ~ 2.4 , which is independent of temperature and field. Second, zero-field spectra give a constant Γ of $\sim 0.94 \text{ meV}$ (Supplementary Fig. 2), but data in field have to be fitted with an increasing Γ as the field is increased (Supplementary Fig. 3). Third, the temperature dependence of the superconducting energy gap can be fitted well with the BCS theory (Fig. 2d), and the observed $2\Delta_0/k_B T_c = 4$ ($\Delta_0 = 1.93 \text{ meV}$) is consistent with previous reports^{6,9}, indicating that LTO is a medium-coupling BCS superconductor. Moreover, a simple relation of $\Delta(B, T)/\Delta(0T, T) \sim -[B/B_{c2}(T)]^2$, can be used to scale the field-dependent energy gap at different temperatures, for example, $T = 2, 6, 10 \text{ K}$ (Fig. 2e). Accordingly, B_{c2} can be extracted from the point contact spectra with $B_{c2}(2\text{K}) \sim 16 \text{ T}$.

We also employed a two-channel method derived from the BTK model to fit our experimental data²⁴. In this method, the pair-breaking effect by field is considered as a normal channel (N) superposed onto the superconducting channel (S). Assuming the differential conductance to take the form $G(h) = h'G_N + (1 - h')G_S$ with $h = B/B_{c2}$, the normalized differential conductance in field should obey the polynomial form $\frac{G(h)}{G_N} = h^r + (1 - h^r)\frac{G_S}{G_N}$, where $\frac{G_S}{G_N}$ is obtained from the BTK model with a constant Γ . The best fitting requires $r = 2$. We note that this value is consistent with those used to fit data for point contacts with other superconductors such as Nb, Mo_3Sb_7 and $\text{Dy}_{0.8}\text{Y}_{0.2}\text{Rh}_4\text{B}_4$ (ref. 24). In this case, the relation, $\Delta(B) \sim -B^2$ emerges again, and the Δ values extracted from the two fitting methods are similar (Fig. 2e). To the best of our knowledge, none of the existing theoretical models can account for the quadratic

relation. When B is close to B_{c2} , the Maki formula²⁵ can be analytically expressed as $|\bar{\Delta}|^2 \sim \frac{B_{c2} - B}{\Psi_2(\frac{1}{2} + \frac{1}{2\pi k_B T})}$, where $\bar{\Delta}$ represents the averaged energy gap taking into account the effect of vortices, and Ψ_2 is the first derivative of the digamma function with A the pair-breaking parameter proportional to B when $B \perp ab$ plane²⁶, but this does not lead to a quadratic field dependence of the superconducting energy gap.

Theoretical model. We note, however, that if there exists an additional anisotropy axis, which breaks the intrinsic symmetry of the system, for example, orbital ordering or a background nematicity, $\Delta(B) \sim -B^2$ can arise. To simplify the discussion without loss of generality, we assume that the superconducting order parameter is a three-component vector, $\Delta = (\Delta_x, \Delta_y, \Delta_z)$. The isotropic gap is then equal to the modulus of this vector: $\Delta_0 = (\Delta\Delta)^{1/2} = (\Delta_x^2 + \Delta_y^2 + \Delta_z^2)^{1/2}$. In zero field, the orientation of the local spin of the Cooper pair changes in real space, while the value of the gap does not change. Therefore, the average magnetic moment of Cooper pairs vanishes, that is, $\langle \Delta(\mathbf{r}) \rangle = 0$. However, in magnetic field \mathbf{B} , the magnetic moments of Cooper pairs can be partially polarized, and therefore the susceptibility χ can develop a paramagnetic component. Thus, we have $\chi_{\text{super}} = \chi_{\text{para}} + \chi_{\text{dia}}$, where the last term is the conventional diamagnetic susceptibility of a superconductor.

The first term χ_{para} should be a function of the magnetic moments of the Cooper pairs, which contributes to the symmetry invariants. There are in general three symmetry invariants here. The first one is just $\Delta\Delta$, the second one is $\Delta\mathbf{B}$. The additional anisotropy axis, for example, orbital ordering or background nematicity associated with some vector \mathbf{b} results in another invariant as $\Delta\mathbf{b}$. In the vicinity of the phase transition, we can use the Taylor expansion to obtain:

$$\chi_{\text{para}}((\Delta\mathbf{b}), (\Delta\mathbf{B})) = \chi_{\text{para}}(0, 0) + \chi'_{\text{para}}(0, 0)(\Delta\mathbf{b}) + \chi'_{\text{para}}(0, 0)(\Delta\mathbf{B}) + (\text{high order terms}) \quad (1)$$

In using this expression, the total free energy of the superconductor in the lowest order with superconducting order parameter can be written in the form:

$$F(\Delta) = \alpha(\Delta\Delta) + 2\delta(\Delta\mathbf{b})(\mathbf{B}\mathbf{B}) + \mu(\mathbf{B}\mathbf{B}) + (\text{high order terms}) \quad (2)$$

Minimization of the free energy with respect to Δ will give the expression $\Delta(B) = (\Delta\Delta)^{1/2} = (-\alpha/2\beta)^{1/2} - \delta b B^2/2|\alpha|$ where α , β and δ are the parameters of the Ginzburg–Landau expansion, and b is the modulus of the vector \mathbf{b} (See Supplementary Note 4 for details). This represents the first plausible explanation giving rise to the relation, $\Delta(B) \sim -B^2$. As for the origin of the symmetry breaking, which gives rise to the vector \mathbf{b} in LTO, we propose that there is an onset of orbital ordering, which takes place in LTO below a transition temperature T_{ch} , arising from orbital degeneracy of t_{2g} sub-band^{27,28}.

We would like to point out that although this relation has not been carefully examined previously, we also observe it in some cuprates, namely, electron-doped $(\text{Nd,Ce})_2\text{CuO}_4$ and $(\text{Pr,L a,Ce})_2\text{CuO}_4$ (Supplementary Fig. 4), indicating the presence of a similar symmetry breaking ordering in these compounds. We believe other ordering mechanisms such as spin stripes or charge density wave may also lead to a symmetry breaking resulting in the vector \mathbf{b} . The electronic nematicity has been widely discussed in hole-doped cuprates^{29,30} and Fe-based superconductors^{31,32} as a competing order to the superconductivity. The exact nature of the ordering in electron-doped cuprates is beyond the scope of the present work³³, but the discovered quadratic relation is perhaps not uncommon across different types of superconductors. On the

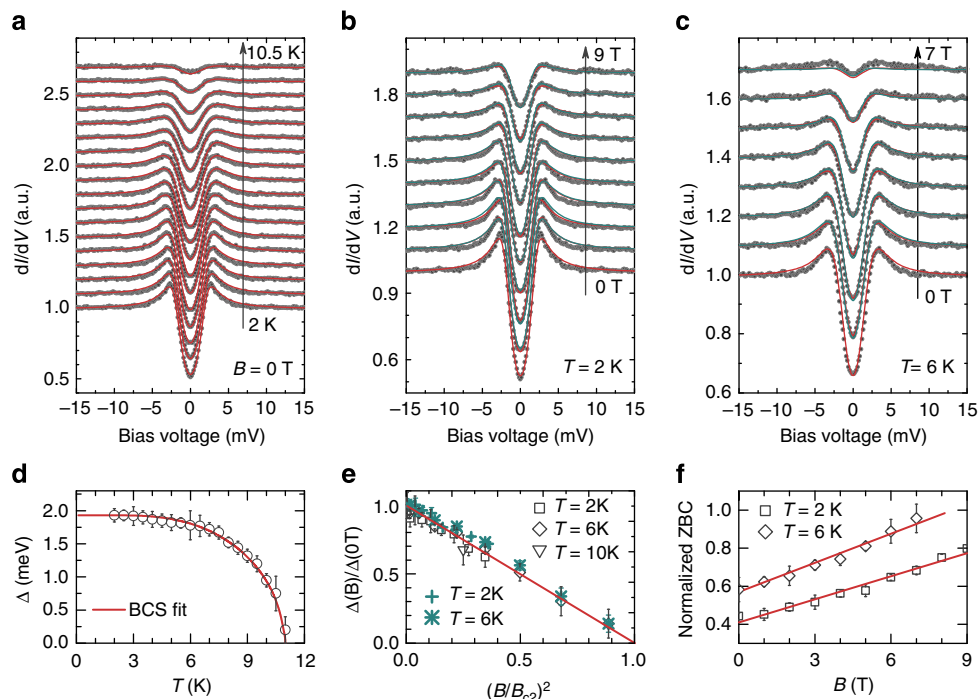


Figure 2 | Temperature- and field-dependent tunnelling spectroscopy curves and the superconducting energy gap of LTO films. (a) Normalized differential conductance versus bias voltage from 2 to 10.5 K ($\Delta T = 0.5$ K) in zero field. Experimental data are fitted with a modified BTK model with a constant broadening Γ term (red lines), and are vertically shifted above the 2 K curve for clarity. (b,c) Normalized differential conductance versus field from 0 to 9 T at 2 K, and from 0 to 7 T at 6 K ($\Delta B = 1$ T, $B \perp ab$ plane). Experimental data (grey circles) are fitted with a modified BTK model with an increasing Γ as B is increased (red lines), and also with the two-channel model (cyan lines). Data in fields are vertically shifted. (d) Temperature-dependent energy gap values, $\Delta(T)$, are obtained from the BTK fits: $2\Delta/k_B T_c = 4$ is obtained, indicating a medium-coupling BCS-like superconductor. (e) Normalized energy gap ($\Delta(B)/\Delta(0T)$) decreases as $(B/B_{c2})^2$ in the superconducting state, and can be scaled for different temperatures. In-field measurements were carried out at $T = 2, 6$ and 10 K (open symbols extracted from modified BTK fittings with an increasing Γ and cross symbols from the two-channel model). (f) The normalized zero bias conductance (symbols) at 2 and 6 K shows a linear dependence on the magnetic field (red straight fitting line). The error bars in d-f represent the s.e. in the fit to the data.

Table 1 | Comparison of physical parameters of LiTi_2O_4 to values from previous work.

	T_c (K)	Δ (meV)	ξ_{BCS} (nm)	ξ_{GL} (nm)	n (cm^{-3})	m^*/m_0	l (nm)	v_F (m s^{-1})	$N(E_F)$
Present	11 ± 0.25	1.93 ± 0.01	14.9	4.47	3×10^{22}	8.11	1.84	1.37×10^5	0.96
Previous	11.5 ± 0.5	1.9	—	4.1–4.6	1.35×10^{22}	9.4	3.2	—	0.97

The quantities in the present work were obtained from transport and tunnelling results on Sample L1. Since most of the earlier studies were carried out on polycrystalline samples, the parameters such as carrier density (n), effective mass (m^*) and density of states ($N(E_F)$; states per eV atom) are from previous magnetic susceptibility measurements using nearly free electron approximations⁷. The mean free path (l) was calculated from the specific heat data⁶. We compare the Ginzburg–Landau coherence length (ξ_{GL}) to the value reported by another thin film study¹⁶, and the superconducting energy gap (Δ) to the value obtained from an Andreev study on polycrystalline samples⁹.

other hand, we note that the relation from the Maki formula is observed in superconductors without symmetry breaking, for example, $\Delta^2(B) \sim -B$ or $-B^2$ for Zn (ref. 34) and $\Delta^2(B) \sim -B$ (Ba,K)BiO₃ (ref. 35). It would therefore be of broad interest to investigate the possible occurrence of the quadratic relation in other superconductors also: it can possibly serve as a signature underpinning different mechanisms leading to intrinsic symmetry breaking, which results in the presence of an additional anisotropy axis.

Zero bias conductance. The normalized zero bias conductance (ZBC) at 2 and 6 K shows a linear dependence on the magnetic field (see Supplementary Note 3 for calculation details), indicating a linear increase of the vortex density with uncorrelated vortices (Fig. 2f). Such a relation has been reported in systems such as $\text{Bi}_2\text{Sr}_2\text{CaCu}_2\text{O}_{8+\delta}$ overdoped with intercalating HgBr_2 molecules³⁶ and in nanosized Pb islands on a silicon wafer³⁷.

The departure from linearity in-field-dependent ZBC has previously been observed in MgB_2 (ref. 38) and $\text{YNi}_2\text{B}_2\text{C}$ (ref. 39), associated with the fact that they are multiband superconductors. In the $\text{Ca}_{2-x}\text{Na}_x\text{CuO}_2\text{Cl}_2$ ($x = 0.14$), the field dependence scales as $B \log B$, suggested to be an indication of a dirty d -wave superconductor⁴⁰. Previous specific heat experiments have suggested that LTO is an s -wave superconductor⁶. Thus, based on the lack of departure from the linearly dependent ZBC, we conclude that LTO is not likely to be a multiband superconductor.

Calculated key physical quantities. Combining the transport and tunnelling data, we were able to extract key parameters for LTO. The Ginzburg–Landau coherence length, the size of the vortex core in type II superconductor is estimated to be $\xi_{\text{GL}} = (\frac{\Phi_0}{2\pi B_{c2}})^{1/2} = 4.47$ nm. The mean free path of $l = 1.8$ nm is

deduced from the Drude model $\rho_0 = \frac{\hbar k_F}{ne^2 l}$, where the Fermi wave vector $k_F = (3\pi^2 n)^{1/3} = 0.96 \text{ \AA}^{-1}$. Since $l < \xi_{\text{GL}}$, the BCS coherence length of $\xi_{\text{BCS}} = 14.9 \text{ nm}$ is calculated from the dirty limit relation, $\xi_{\text{GL}} = \frac{0.855 \times (\xi_{\text{BCS}})^{1/2}}{(1 - T/T_c)^{1/2}}$. We then calculate the Fermi velocity from the formula, $\xi_{\text{BCS}} = \hbar v_F / \pi \Delta$, and arrive at an effective mass of $m^*/m_0 = 8.11$ (with m_0 being the free electron mass), and the density of states at the Fermi level is found to be $N(E_F) = 0.96$ states per eV atom.

We compared these parameters to those obtained from previous reports on LTO. Only T_c and ξ_{GL} values have been previously reported on thin films¹⁶, and the other quantities were from the magnetic susceptibility⁷, Andreev reflection⁹ and specific heat⁶ measurements on polycrystalline samples. As seen in Table 1, the values obtained in the present work are consistent with those from previous reports. We note that in polycrystalline samples, the grain boundaries prevent accurate calculations from the transport measurements due to boundary scattering, but the parameters could be extracted from heat capacity and susceptibility data. These values indicate that the nearly free electron model can capture the main physics of the LTO system.

Field direction dependence of magnetoresistivity. In the normal state, we observe an anomalous MR behaviour. Figure 3a illustrates the field-dependent MR in sample L1 when $B \perp ab$ plane. The MR gradually decreases from positive to negative with increasing temperature, and a crossover is observed at $50 \pm 10 \text{ K}$. In the inset of Fig. 3a, the MR is plotted as B^2 . The positive MR is proportional to B^2 , whereas the negative MR is not. In the case of $B \perp ab$ plane, both orbital and spin effects can contribute to MR, and in order to discern the different contributions additional measurements were carried out where the field was also applied in the film plane with $B // I$ (parallel to current) and $B \perp I$ (normal to current). In Fig. 3b, the temperature dependence of MR is plotted for both L1 (grey symbols) and L2 (red symbols). The negative MR is nearly independent of the field directions, but the positive MR displays unambiguous anisotropy, that is, $\text{MR}(B \perp ab \text{ plane}) > \text{MR}(B // ab \text{ plane}, B \perp I) > \text{MR}(B // ab \text{ plane} // I)$. Moreover, the MR changes its sign when $B // I$, as seen in Fig. 4a. The first derivative of $\rho_{xx}(T)$ in zero field (symbols) starts to deviate from the Fermi liquid behaviour ($d\rho_{xx}/dT \sim T$) at roughly the same range of temperature as seen in Fig. 4b, indicating the presence of an enhanced electron–electron interaction.

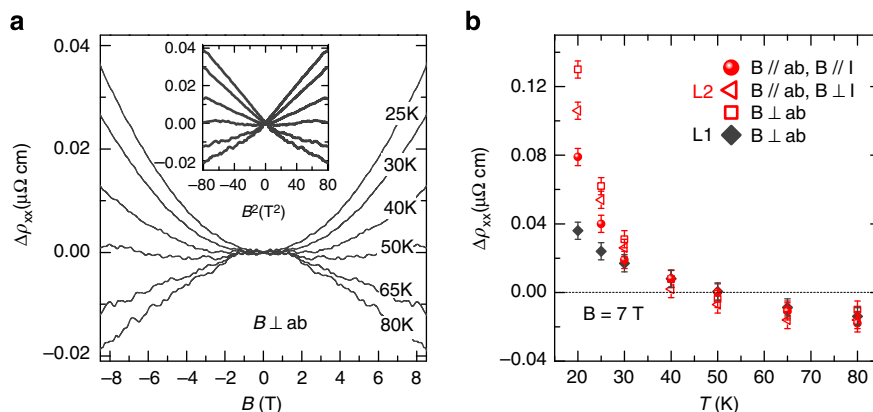


Figure 3 | Temperature dependence of magnetoresistivity. (a) The transverse magnetoresistivity with $B \perp ab$ plane, $\Delta\rho_{xx} = \rho_{xx}(B) - \rho_{xx}(0T)$, changes from negative to positive as temperature is decreased. The crossover temperature is $\sim 50 \pm 10 \text{ K}$. The positive magnetoresistivity is proportional to B^2 as seen in the inset, whereas the negative MR is not. (b) Magnetoresistivity at 7 T plotted against the temperature. The dark and red symbols are for samples L1 and L2, respectively. The magnetic field was applied along three different directions, that is, $B // ab$ plane ($B // I$, $B \perp I$) and $B \perp ab$ plane. The error bars are maximum data noise in determining the magnetoresistivity. The negative magnetoresistivity is nearly isotropic, whereas the positive magnetoresistivity shows unambiguous anisotropy.

Such transport data collectively point to the presence of a phase transition or crossover with a characteristic temperature T_{ch} of $\sim 50 \pm 10 \text{ K}$. As discussed above, we believe orbital ordering results in the relation, $\Delta(B) \sim -B^2$. Thus, we associate T_{ch} with the onset of an orbital-related state such as orbital ordering or nematicity (see Supplementary Note 4). If the LTO system indeed has such a symmetry breaking feature, it should also manifest itself in the anisotropy of the in-plane angular-dependent magnetoresistivity (AMR) measurements, and a twofold symmetry would be expected, similar to the case of iron arsenide superconductors⁴¹. We indeed observe a twofold AMR in LTO (Fig. 4c). Note that a strong enhancement in amplitude of the twofold symmetry takes place below T_{ch} : we associate this with the orbital-related ordering. On the other hand, we find that the starting temperature of the twofold AMR is $\sim 100 \pm 10 \text{ K}$, far above the T_{ch} .

Temperature dependence of magnetic susceptibility. To understand this unusual behaviour, we also measured the temperature-dependent susceptibility in zero field and field cooling. The $\chi(T)$ in zero-field cooling data shows a clear screening effect due to superconductivity $< 11 \text{ K}$ (Fig. 4e). In-field cooling, we find that the residual susceptibility, $\delta\chi(T)$, found by subtracting a paramagnetic component from the $\chi(T)$, starts to increase below $100 \pm 10 \text{ K}$ (Fig. 4d), corresponding to the same temperature where the twofold symmetry emerges. The amplitude of the twofold symmetry exhibits an abrupt increase at $T_{\text{ch}} = 50 \pm 10 \text{ K}$. We, thus, attribute the twofold AMR to two sources: one related to a spin interaction starting at a higher temperature ($100 \pm 10 \text{ K}$), and the other associated with an orbital effect (discussed below) becoming pronounced below $T_{\text{ch}} = 50 \pm 10 \text{ K}$.

Discussion

Our findings, thus far, can be summarized in the following three points: (1) With decreasing temperature, the magnetic susceptibility increases and deviates from the Curie–Weiss behaviour $< 100 \pm 10 \text{ K}$, while the in-plane AMR starts to show a twofold symmetry and the magnetoresistivity is negative in field; (2) At $T_{\text{ch}} \sim 50 \pm 10 \text{ K}$, the sign of magnetoresistivity changes to positive and the twofold symmetry becomes more prominent, where we also observe deviation from the Fermi liquid behaviour; (3) Below 11 K, LTO enters the superconducting state, where the superconducting energy gap decreases as a function of B^2 .

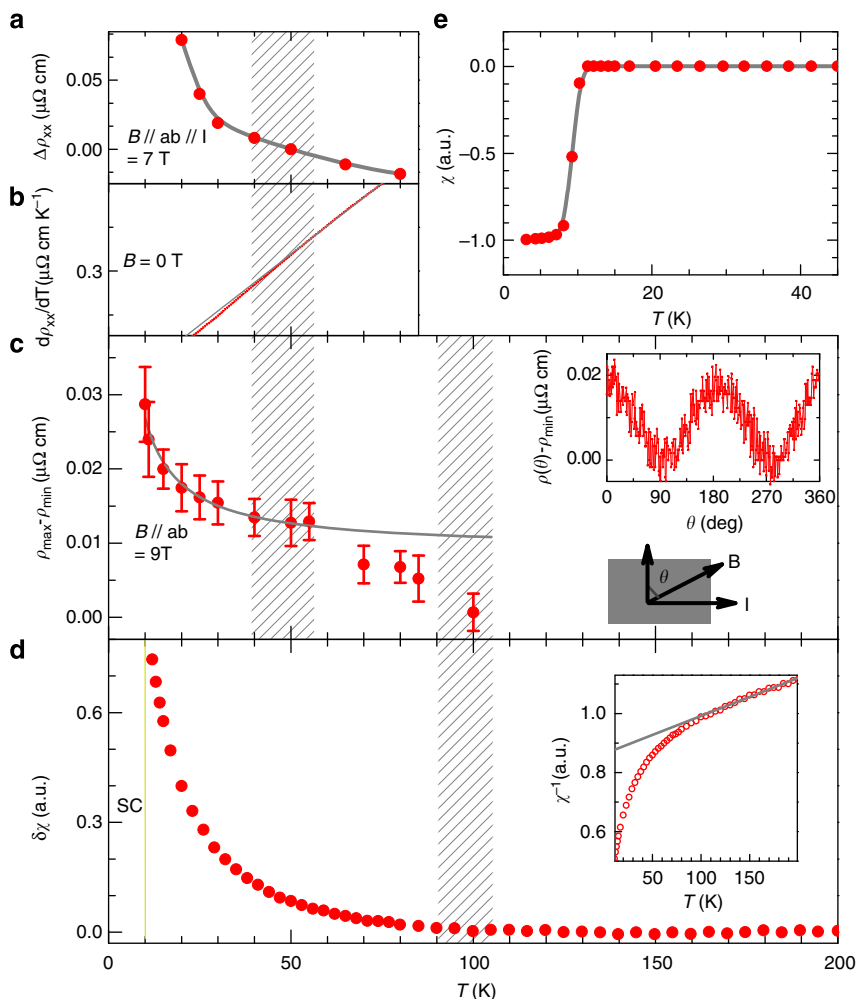


Figure 4 | Magnetoresistivity and susceptibility features of LiTi_2O_4 thin films. (a) Temperature-dependent longitudinal magnetoresistivity ($B//ab$ plane// I), $\Delta\rho_{xx} = \rho_{xx}(B) - \rho_{xx}(0T)$, is replotted to demonstrate the crossover temperature (also see Fig. 3b). (b) $d\rho_{xx}/dT$ in zero field. It deviates from the Fermi liquid behaviour, $d\rho_{xx}/dT \sim T$ (grey line), at lower temperatures. (c) Twofold symmetry of in-plane (ab plane) resistivity, where ρ_{\max} ($\theta = 90^\circ$) and ρ_{\min} ($\theta = 0^\circ$) are found from plots such as indicated in the inset. The inset shows a typical twofold symmetry at 30 K and 9 T against θ , which is the angle between the normal direction to current and the field. The error bars are maximum data noise as seen in the inset. (d) The susceptibility with field cooling (1,000 Oe, $B//ab$ plane) shows a Curie-Weiss behaviour at high temperature (see inset $\chi^{-1}(T)$). We plot the residual susceptibility $\delta\chi$ as a function of temperature after subtracting the paramagnetic contribution. The $\delta\chi$ starts to increase below 100 ± 10 K, coincident with the starting temperature of the twofold symmetry of in-plane resistivity. (e) The susceptibility with zero-field cooling shows a good superconducting screening signal, suggesting our LTO films are of high quality. The shading areas around 100 K and 50 K represent the uncertainties in defining the starting point of the anisotropic AMR and the abrupt increase, respectively.

Generally, MR can result from charge, orbital or spin interactions, as well as interactions among them⁴². The observed constant Hall coefficient and smooth temperature evolution of the c -axis lattice parameter (Supplementary Fig. 8) preclude the presence of charge density waves, which normally influences the Hall coefficient⁴³. The mean free path of the ‘clean’ sample (L1) is 1.84 nm in the zero-temperature limit, which is only about two unit cells of the LTO lattice. Therefore, a grain boundary effect is unlikely to have a dominant role in the MR behaviour. The combination of points (2) and (3) above supports an orbital effect as the origin of the positive anisotropic MR below 50 ± 10 K, which introduces the additional anisotropic axis in the system used in the theoretical model. The temperature at which the twofold AMR at 100 ± 10 K emerges corresponds to the temperature where the increase in antiferromagnetic-like spin correlation takes place (and where the Curie-Weiss fitting intercepts the temperature axis at negative value), indicating that the negative MR is associated with a spin interaction.

We note that in $\text{La}_{2-x}\text{Ce}_x\text{CuO}_4$ thin films, antiferromagnetism (AFM) has been identified as the main cause of a twofold symmetry of AMR and a negative MR⁴⁴, while in Fe-based superconductors the anisotropy of in-plane charge transport was found to be associated with a nematic order⁴¹. Though the spinel structure is different from the perovskite one, we believe it is not unreasonable to link the appearance of a twofold symmetry of AMR at 100 ± 10 K to local AFM spin correlations, and the sudden enhancement at 50 ± 10 K to an orbital related state.

In antiferromagnetic metals, a sign change in MR is expected theoretically at the Neel temperature due to the s - d electron interaction⁴⁵. However, this idea is based on long range AFM, and the change in sign from negative to positive is to be accompanied by a discontinuous jump in MR. This is in contrast to the observation in LTO, where there is no discontinuous jump. Moreover, the LTO system has a frustrated Ti sublattice containing equal numbers of Ti^{3+} and Ti^{4+} , and thus a long range AFM ordering is unfavourable¹². The emergence of

short-range AFM ordering has been reported in V-doped LTO by nuclear magnetic resonance¹¹ and in LiV_2O_4 by inelastic neutron scattering⁴⁶. Note that the AMR measurements cannot be used to tell whether the AFM is static or dynamic. It is possible that local spin fluctuations are responsible for the negative MR.

We consider an alternative explanation due to the effect of spin-orbit coupling. When the orbital ordered (nematic) state is destroyed at $T > T_{\text{ch}}$, some ‘fluctuating’ islands may have a finite lifetime and serve as additional (magnetic) scattering centres for the electron transport. When the magnetic field is applied, some of these islands disappear and the resistivity decreases. This is exemplified in thin metallic Mg films covered with small controlled quantities of a magnetic ion such as Fe or a heavy ion with large spin-orbit coupling such as Au: the magnetoresistance changes its sign from negative to positive on experiencing an increase in the number of spin-orbit scattering centres⁴⁷. Perhaps a similar mechanism is at work in LTO.

In conclusion, detailed properties of superconducting LTO were investigated for the first time in high quality thin films. Many properties are consistent with previous work on polycrystalline samples: we observe one type of charge carrier and a $\frac{2\Delta}{k_B T_c}$ value consistent with a medium-coupling BCS superconductor. The main physics can be captured by the nearly free electron model. However, we find two new and distinct features in this system. In the superconducting state, a scaling law, $\Delta(B) \sim -B^2$ at $T < T_c$, is extracted from our point contact spectra. This behaviour had not been predicted by any previous theory. In the normal state, an anomalous MR, which crosses over from nearly isotropic negative MR to an anisotropic positive MR with decreasing temperature, is observed. The anisotropic positive MR likely originates from the enhanced electron-electron interaction due to the orbital related ordering below $T_{\text{ch}} \sim 50 \pm 10$ K. The negative MR occurring at 100 ± 10 K possibly stems from the suppression of spin-orbit scattering or local spin fluctuations. We present a new theoretical model based on the proposal that there is orbital ordering in the superconducting state to account for the relation $\Delta(B) \sim -B^2$. The fact that this relation is also observed in other materials ($(\text{Nd,Ce})_2\text{CuO}_4$ and $(\text{Pr,L a,Ce})_2\text{CuO}_4$) points to the broader applicability of the model developed here in understanding underlying interactions in different types of superconductors.

References

- Moshopoulou, E. G. Superconductivity in the spinel compound LiTi_2O_4 . *J. Am. Ceram. Soc.* **82**, 3317–3320 (1999).
- Johnston, D. C., Prakash, H., Zacharia, Wh & Viswanat, R. High-temperature superconductivity in Li-Ti-O Ternary system. *Mater. Res. Bull.* **8**, 777–784 (1973).
- Massidda, S., Yu, J. J. & Freeman, A. J. Electronic-structure and properties of superconducting LiTi_2O_4 . *Phys. Rev. B* **38**, 11352–11357 (1988).
- Satpathy, S. & Martin, R. Electronic structure of the superconducting oxide spinel LiTi_2O_4 . *Phys. Rev. B* **36**, 7269–7272 (1987).
- Johnston, D. C., Swenson, C. A. & Kondo, S. Specific heat (1.2–108 K) and thermal expansion (4.4–297 K) measurements of the 3d heavy-fermion compound LiV_2O_4 . *Phys. Rev. B* **59**, 2627–2641 (1999).
- Sun, C. P. *et al.* Magnetic field dependence of low-temperature specific heat of the spinel oxide superconductor LiTi_2O_4 . *Phys. Rev. B* **70**, 054519 (2004).
- Johnston, D. C. Superconducting and normal state properties of spinel compounds. I. Preparation, crystallography, superconducting properties, electrical resistivity, dielectric behaviour, and magnetic susceptibility. *J. Low Temp. Phys.* **25**, 145–175 (1976).
- Tunstall, D. P. *et al.* Titanium nuclear magnetic resonance in metallic superconducting lithium titanate and its lithium-substituted derivatives $\text{Li}_{1-x}\text{Ti}_{2-x}\text{O}_4$ ($0 < x < 0.10$). *Phys. Rev. B* **50**, 16541–16549 (1994).
- Tang, L. *et al.* Electrical resistivity and Andreev reflection spectroscopy of the superconducting oxide spinel LiTi_2O_4 . *Phys. Rev. B* **73**, 184521 (2006).
- Chen, C. L. *et al.* Role of 3d electrons in the rapid suppression of superconductivity in the dilute V doped spinel superconductor LiTi_2O_4 . *Supercond. Sci. Technol.* **24**, 115007 (2011).
- Itoh, Y., Moritsu, N. & Yoshimura, K. Emergence of antiferromagnetic correlation in $\text{LiTi}_{2-x}\text{V}_x\text{O}_4$ via ^7Li NMR. *J. Phys. Soc. Jpn* **77**, 123713 (2008).
- Anderson, P. W. Ordering and antiferromagnetism in ferrites. *Phys. Rev.* **102**, 1008–1013 (1956).
- Jin, K., Butch, N. P., Kirshenbaum, K., Paglione, J. & Greene, R. L. Link between spin fluctuations and electron pairing in copper oxide superconductors. *Nature* **476**, 73–75 (2011).
- Paglione, J. & Greene, R. L. High-temperature superconductivity in iron-based materials. *Nat. Phys.* **6**, 645–658 (2010).
- Inukai, T., Murakami, T. & Inamura, T. Preparation of superconducting LiTi_2O_4 thin films. *Thin Solid Films* **94**, 47–50 (1982).
- Chopdekar, R. V. *et al.* Growth and characterization of superconducting spinel oxide LiTi_2O_4 thin films. *Physica C* **469**, 1885–1891 (2009).
- Kumatani, A. *et al.* Growth processes of lithium titanate thin films deposited by using pulsed laser deposition. *Appl. Phys. Lett.* **101**, 123103 (2012).
- Diamant, I., Hacohen-Gourgy, S. & Dagan, Y. Evolution of a bosonic mode across the superconducting dome in the high- T_c cuprate $\text{Pr}_{2-x}\text{Ce}_x\text{CuO}_{4-\delta}$. *Phys. Rev. B* **84**, 104511 (2011).
- Blonder, G. E., Tinkham, M. & Klapwijk, T. Transition from metallic to tunnelling regimes in superconducting microconstrictions: excess current, charge imbalance, and supercurrent conversion. *Phys. Rev. B* **25**, 4515–4532 (1982).
- Blonder, G. E. & Tinkham, M. Metallic to tunnelling transition in Cu-Nb point contacts. *Phys. Rev. B* **27**, 112–118 (1983).
- Dynes, R., Garno, J., Hertel, G. & Orlando, T. Tunnelling study of superconductivity near the metal-insulator transition. *Phys. Rev. Lett.* **53**, 2437–2440 (1984).
- Bandte, C., Hertel, P. & Appel, J. Pair-breaking effects in high-temperature superconductors. *Phys. Rev. B* **45**, 8026–8035 (1992).
- Daghero, D. & Gonnelli, R. S. Probing multiband superconductivity by point-contact spectroscopy. *Supercond. Sci. Technol.* **23**, 043001 (2010).
- Smith, C. W. & Dolan, P. J. Determining transport parameters for superconductor/normal metal point contacts at fixed temperature from conductance versus magnetic field data. *Physica C* **471**, 285–289 (2011).
- Maki, K. Pauli paramagnetism and superconducting state II. *Prog. Theor. Phys.* **32**, 29–36 (1964).
- Tinkham, M. *Introduction to Superconductivity* (2nd edn, Ch. 10. Mineola, 2004).
- Laad, M. S., Bradarić, I. & Kusmartsev, F. V. Orbital non-Fermi-liquid behaviour in cubic ruthenates. *Phys. Rev. Lett.* **100**, 096402 (2008).
- Kusmartsev, F.V. Formation of electron strings in narrow band polar semiconductors. *Phys. Rev. Lett.* **84**, 530–533 (2000).
- Daou, R. *et al.* Broken rotational symmetry in the pseudogap phase of a high- T_c superconductor. *Nature* **463**, 519–522 (2010).
- Vojta, M. Lattice-symmetry breaking in cuprate superconductors: stripes, nematics and superconductivity. *Adv. Phys.* **58**, 699–820 (2009).
- Baek, S.-H. *et al.* Orbital-driven nematicity in FeSe. *Nat. Mater.* **14**, 210–214 (2015).
- Kontani, H. & Yamakawa, Y. Linear response theory for shear modulus C_{66} and Raman quadrupole susceptibility: evidence for nematic orbital fluctuations in Fe-based superconductors. *Phys. Rev. Lett.* **113**, 047001 (2014).
- Armitage, N. P., Fournier, P. & Greene, R. L. Progress and perspectives on the electron-doped cuprates. *Rev. Mod. Phys.* **82**, 2421–2487 (2010).
- Naidyuk, Y. G., Löhneysen, H.v. & Yanson, I. K. Temperature and magnetic-field dependence of the superconducting order parameter in Zn studied by point-contact spectroscopy. *Phys. Rev. B* **54**, 16077–16081 (1996).
- Szabó, P. *et al.* Magnetic pair breaking in superconducting $\text{Ba}_{1-x}\text{K}_x\text{BiO}_3$ investigated by magnetotunneling. *Phys. Rev. B* **62**, 3502–3507 (2000).
- Krasnov, V. M., Kovalev, A. E., Yurgens, A. & Winkler, D. Magnetic field dependence of the superconducting gap and the pseudogap in Bi2212 and HgBr2-Bi2212 , studied by intrinsic tunnelling spectroscopy. *Phys. Rev. Lett.* **86**, 2657–2660 (2001).
- Ning, Y. X. *et al.* Observation of surface superconductivity and direct vortex imaging of a Pb thin island with a scanning tunnelling microscope. *Europhys. Lett.* **85**, 27004 (2009).
- Eskildsen, M. R. *et al.* Scanning tunnelling spectroscopy on single crystal MgB_2 . *Physica C* **385**, 169–176 (2003).
- Mukhopadhyay, S., Sheet, G., Raychaudhuri, P. & Takeya, H. Magnetic-field dependence of superconducting energy gaps in $\text{YNi}_2\text{B}_2\text{C}$: evidence of multiband superconductivity. *Phys. Rev. B* **72**, 014545 (2005).
- Hanaguri, T. *et al.* Coherence factors in a high- T_c cuprate probed by quasi-particle scattering off vortices. *Science* **323**, 923–926 (2009).
- Chu, J. H. *et al.* In-plane resistivity anisotropy in an underdoped iron arsenide superconductor. *Science* **329**, 824–826 (2010).
- Imada, M., Fujimori, A. & Tokura, Y. Metal-insulator transitions. *Rev. Mod. Phys.* **70**, 1039–1263 (1998).
- Daou, R. *et al.* Linear temperature dependence of resistivity and change in the Fermi surface at the pseudogap critical point of a high- T_c superconductor. *Nat. Phys.* **5**, 31–34 (2009).

44. Jin, K. *et al.* Evidence for antiferromagnetic order in $\text{La}_{2-x}\text{Ce}_x\text{CuO}_4$ from angular magnetoresistance measurements. *Phys. Rev. B* **80**, 012501 (2009).
45. Yamada, H. & Takada, S. Magnetoresistance of antiferromagnetic metals due to s-d interaction. *J. Phys. Soc. Jpn.* **34**, 51–57 (1973).
46. Lee, S. H., Qiu, Y., Broholm, C., Ueda, Y. & Rush, J. Spin fluctuations in a magnetically frustrated metal LiV_2O_4 . *Phys. Rev. Lett.* **86**, 5554–5557 (2001).
47. Bergman, G. Measurement of the magnetic scattering time by weak localization. *Phys. Rev. Lett.* **49**, 162–164 (1982).

Acknowledgements

We would like to thank Y. Dagan, Y. Nakajima, J. Paglione, P. Dai, G. Zheng, K. Liu and Z. Meng for useful discussions. This research was supported by the National Science Foundation (DMR-1104256 and 1410665), AFOSR-MURI (FA9550-09-1-0603), AFOSR (FA95501410332), the Strategic Priority Research Program (B) of the Chinese Academy of Sciences (XDB07020100) and the National Natural Science Foundation of China Grant (11474338, 11322432).

Author contributions

K.J., R.L.G. and I.T. designed the research; S.M., S.Y., R.S. and J.S. prepared the thin films; K.J. performed transport and point contact measurements; X.Z., Y.J., H.S.Y. and J.Y. complemented transport measurements; K.J., G.H., L.S., F.V.K. and R.L.G. analysed the data; K.J., R.L.G. and I.T. wrote the paper.

Additional information

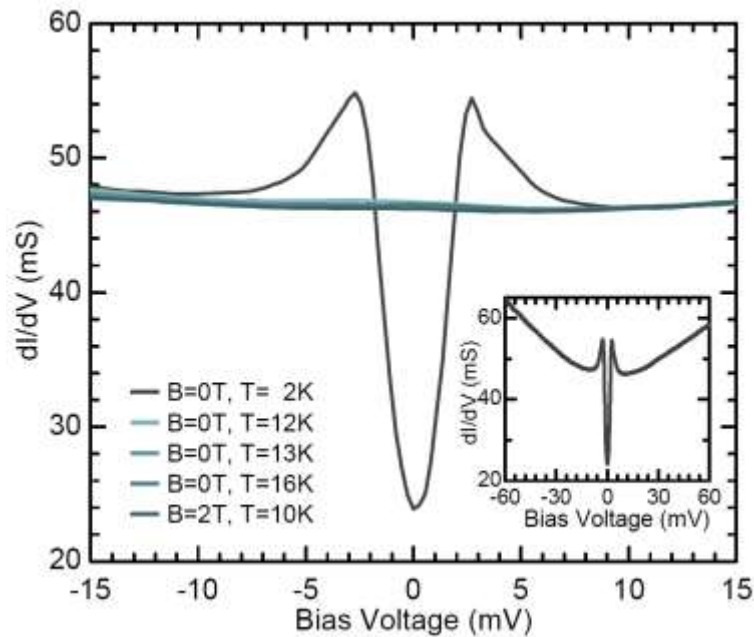
Supplementary Information accompanies this paper at <http://www.nature.com/naturecommunications>

Competing financial interests: The authors declare no competing financial interests.

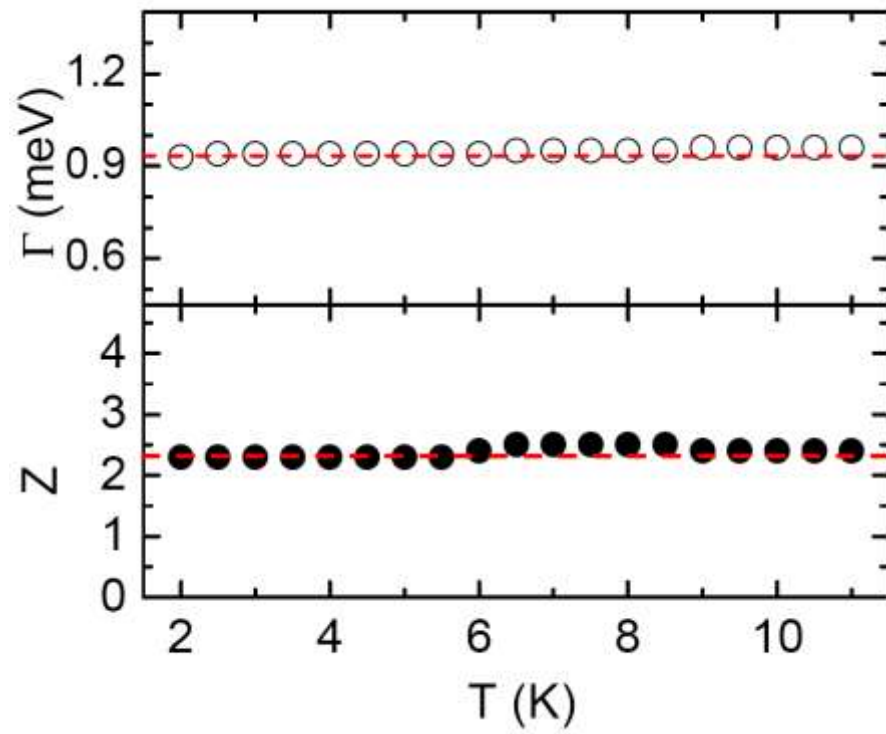
Reprints and permission information is available online at <http://npg.nature.com/reprintsandpermissions/>

How to cite this article: Jin, K. *et al.* Anomalous magnetoresistance in the spinel superconductor LiTi_2O_4 . *Nat. Commun.* **6**:7183 doi: 10.1038/ncomms8183 (2015).

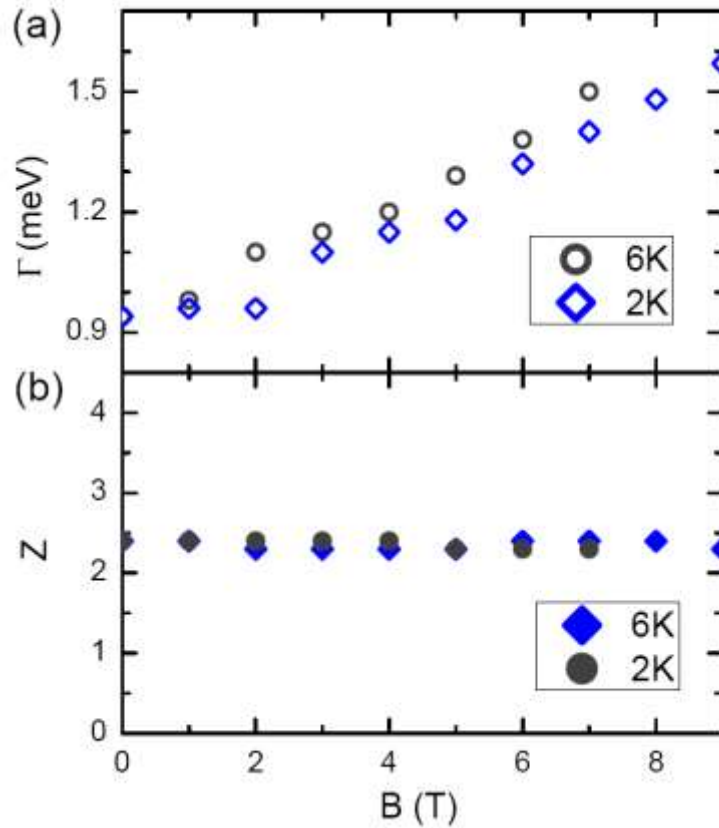
Supplementary Figures



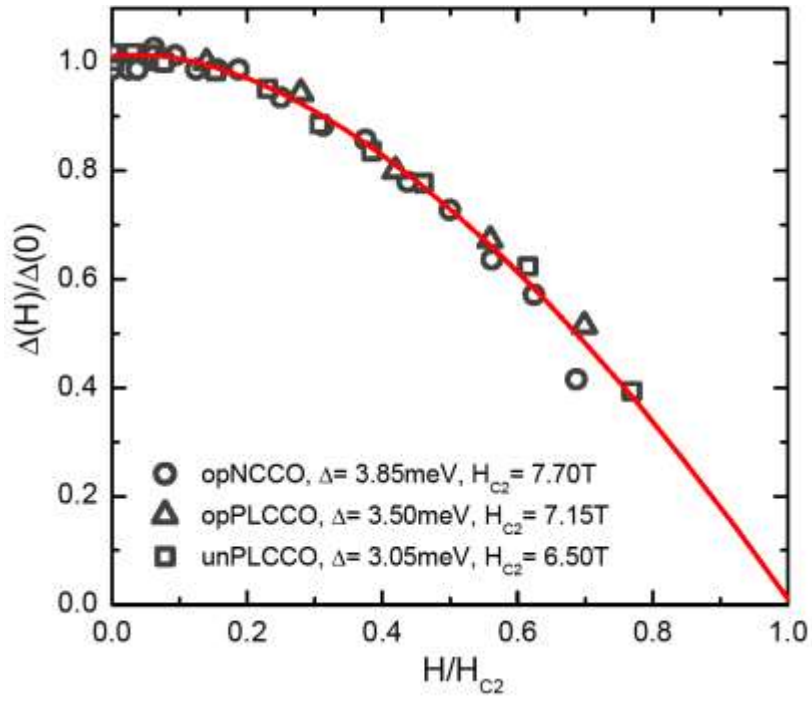
Supplementary Figure 1 | Point-contact spectra of a Pt-Ir tip/LTO film junction. The main panel shows differential conductance at 2, 12, 13, 16 K (0 T), and 10 K (2 T) to demonstrate the normalization procedure. The inset shows the raw spectrum data at 2 K in zero field.



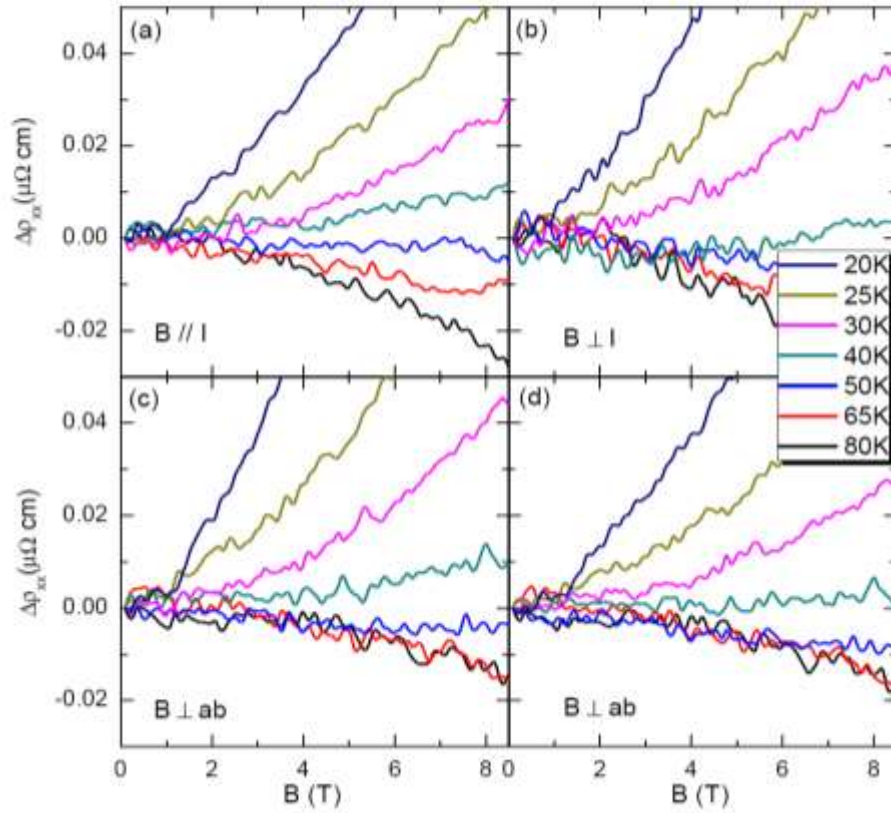
Supplementary Figure 2| Temperature dependence of fitting parameters, Γ and Z , in zero magnetic field.



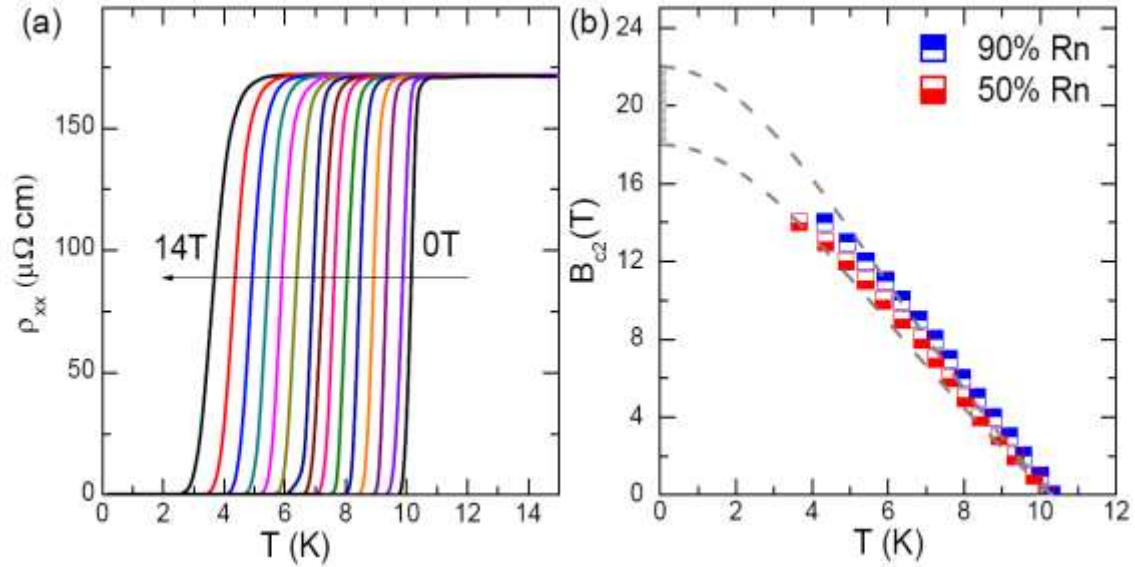
Supplementary Figure 3| Field dependence of fitting parameters, Γ and Z , at 2K and 6 K. Z is constant but Γ increases with increasing field, extracted from the red fitting curves shown in Figures 2b and 2c in the main text. Here, the enhancement of Γ is due to the pair-breaking effect by field.



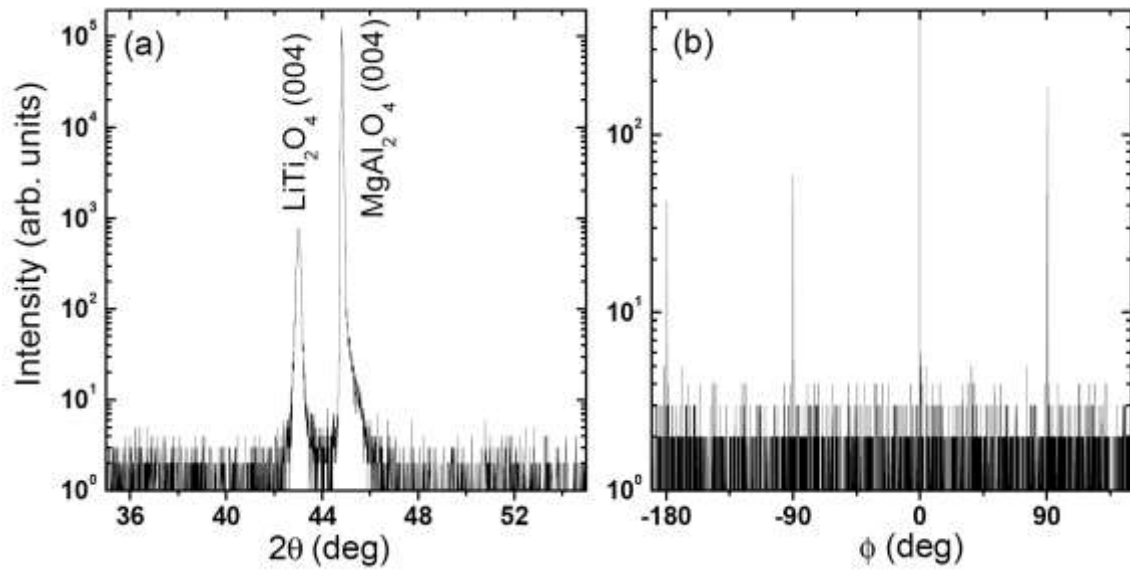
Supplementary Figure 4| Magnetic field dependence of superconducting energy gap of optimal-doped (op) of NCCO, PLCCO and under-doped (un) PLCCO systems. The experimental data (symbols) obey $\Delta(H)/\Delta(0) = 1 - (H/H_{c2})^2$ (red line).



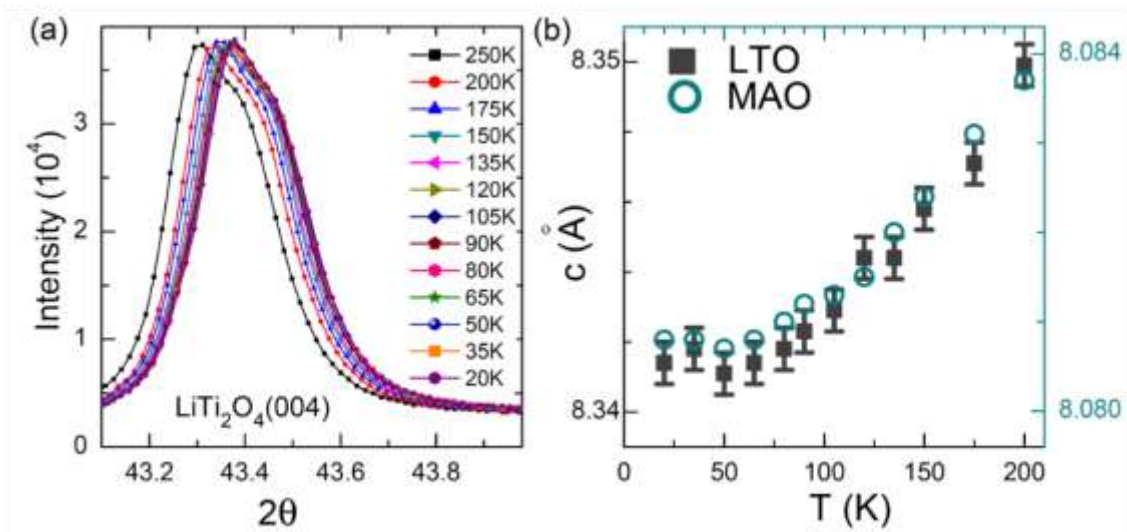
Supplementary Figure 5| Magnetoresistivity versus temperature with different field directions on sample L2. The magnetic field was applied along three different directions, i.e., in the ab -plane with $B // I$ (a), $B \perp I$ (b) and $B \perp ab$ plane (c) (d). (c) (d) show data taken from different parts of the same sample L2.



Supplementary Figure 6| Resistivity and upper critical field of the sample L2. (a) $\rho(T)$ in fields ($B \perp ab$ plane) shows that even 14 Tesla cannot suppress the superconductivity. (b) Upper critical fields defined as the values of 90% and 50% of normal state resistivity (R_n) plotted against the temperature. The experimental data can be fitted by $B_{c2}(T) = B_{c2}(0)[1 - (T/T_c)^2]/[1 + (T/T_c)^2]$ derived from the Ginzburg-Landau theory.



Supplementary Figure 7 | X-ray diffraction of LTO thin films. (a) The θ - 2θ scan indicates *c*-axis oriented growth. (b) The ϕ -scan of the (404) reflection.



Supplementary Figure 8| Temperature dependence of X-ray diffraction data and lattice parameters. (a) LTO (004) peak at different temperatures. (b) Temperature dependent c -axis parameter values for both the LTO film and the MgAl_2O_4 (MAO) substrate were extracted from X-ray diffraction measurements. They both shrink gradually as temperature decreases. The rate of change with temperature (thermal expansion) is roughly consistent with previous reports on bulk materials^{13, 14}.

Supplementary Note 1

Method to normalize the tunneling spectra

In point-contact spectroscopy measurements, the actual measured voltage is comprised of the signal from the junction (dV/dI) in series with a sample resistance (R_s). In the superconducting (SC) state R_s equals zero, while in the non-SC state, the contribution from R_s has to be removed before carrying out the normalization. At low temperatures, the upper critical field of LiTi_2O_4 (LTO) is beyond the applied magnetic field in this experiment, so we choose the normal state spectra either at $T > T_c$ or at $B > B_{c2}$ as the reference to normalize the spectra below T_c . From the main text, it can be seen that the resistivity of LTO is almost flat at low T . This is why the spectra overlap with each other at 10 K (2 T), 12, 13, 16 K (0 T), and thus can be used as references to normalize the spectra below T_c (see Supplementary Figure 1). The normalized data were obtained via

$$(dV/dI)_{\text{normalized}} = \frac{(dV/dI)_s}{(dV/dI)_N - R_s} \quad (1)$$

where $(dV/dI)_s$ represents data below T_c , and $(dV/dI)_N$ refers to the data at 10 K (2 T), 12, 13, 16 K (0 T). Meanwhile, $V = V_m - IR_s$, with V_m the applied bias voltage and V the actual bias on the junction. According to the BTK theory, the normalized dV/dI should be equal to 1 at high bias, namely

$$\left(\frac{dV}{dI}\right)_s \Big/ \left[\left(\frac{dV}{dI}\right)_N - R_s\right] = 1 \quad (2)$$

Then we can get the sample resistance R_s and also the normalized conductance (Figure 2 in the main text). The raw data of differential conductance at 2 K and 0 T are shown in the inset of Supplementary Figure 1 as a function of the bias voltage up to 60 mV. An asymmetrical background appears at higher bias which also has been observed previously in other superconducting systems¹. We symmetrized the raw spectrum by averaging the signal in negative and positive bias. Note that the asymmetry at lower bias is small, and the uncertainty in determining the fitting parameters is straightforward and contained in the error bars in all the related Figures.

Supplementary Note 2

Fitting parameters

We use the BTK theory to fit the tunneling spectra data, which contain three parameters (Δ , Z , Γ). The Z and Γ are constant for changing temperature in zero field as seen in Supplementary Figure 3. In fields, two methods were used to fit the spectra, i.e., the two-channel model² and the modified BTK model with an enhanced Γ in field³.

When a two-channel model derived from the BTK model was used to fit the spectra, a roughly constant Γ was used because the pair-breaking effect by field was separated and expressed as a normal channel superposed onto the superconducting channel. However, if the effect due to field was taken as a part of contribution to Γ , then we found the Γ increased with increasing the field (see Supplementary Figure 3). In general, pair-breaking processes result in a smearing of the DOS at the gap edges, similar to the DOS in the modified BTK theory described by $E' = E + i\Gamma$. Regardless of the method used, we always arrive at the simple relation $\Delta \sim B^2$.

Supplementary Note 3

Zero bias conductance

The normalized zero bias conductance (ZBC) is given by

$$\frac{\sigma}{\sigma_N}(V=0) = (1+Z^2) \int dE [1+A(E)-B(E)] \left(-\frac{\partial f(E+eV)}{\partial V} \right) \Bigg|_{V=0} \quad (3)$$

where $f(E)$, $A(E)$, and $B(E)$ represent the Fermi distribution, probability of Andreev reflection, and the probability of ordinary reflection, respectively. Note that the intrinsic ZBC should be obtained as $Z \rightarrow \infty$. Going to a larger Z will reduce the normalized ZBC very little as $Z > 1.5$ (ref. 4). In our calculations, the reduction by larger Z was negligible since $Z = 2.4$ in our case, as seen in Figure 2f in the main text.

The normalized ZBC at 2 K and 6 K shows a linear dependence on the magnetic field (see Fig. 2f in the main text), indicating a linear increase of the vortex density with uncorrelated vortices. Such relation has been reported in systems such as overdoped $\text{Bi}_2\text{Sr}_2\text{CaCu}_2\text{O}_{8+\delta}$ (Bi2212 intercalating with HgBr_2 molecules) (ref. 5), nanosized Pb islands on silicon wafer⁶. The departure from the linearity between ZBC and field was observed in MgB_2 (ref. 7) and $\text{YNi}_2\text{B}_2\text{C}$ (ref. 8), which are multiband superconductors. In the $\text{Ca}_{2-x}\text{Na}_x\text{CuO}_2\text{Cl}_2$ ($x = 0.14$), the field dependence goes as $B \log B$, which is suggested to be an indication of dirty d -wave superconductor⁹.

Supplementary Note 4

Quadratic relation between Δ and B

To the best of our knowledge, the quadratic field dependence of the superconducting gap is formally reported for the first time in the present work. As discussed in the main text, the Maki formula will not generate a simple relation $\Delta \sim B^2$ instead, $|\Delta|^2 \sim -B$ would be expected if the pair-breaking factor is a small value compared to $k_B T$. However, if there is an additional anisotropic axis due to symmetry breaking, for example, due to orbital ordering or background nematicity, $\Delta \sim -B^2$ could result as discussed in the following.

To simplify the discussion without loss of generality, we assume that the superconducting order parameter is a 3-component vector, $\mathbf{\Delta} = (\Delta_x, \Delta_y, \Delta_z)$. Then the isotropic gap is equal to the

modulus of this vector: $\Delta_0 = (\mathbf{\Delta} \cdot \mathbf{\Delta})^{1/2} = (\Delta_x^2 + \Delta_y^2 + \Delta_z^2)^{1/2}$. In zero field, the orientation of the local spin of the Cooper pair changes in real space, while the value of the gap does not change. Therefore, the average magnetic moment of Cooper pairs vanishes, that is $\langle \mathbf{\Delta}(\mathbf{r}) \rangle = \mathbf{0}$. However, in magnetic field, \mathbf{B} , the magnetic moments of Cooper pairs can be partially polarized and therefore the susceptibility, χ , can develop a paramagnetic component, so that $\chi_{\text{super}} = \chi_{\text{para}} + \chi_{\text{dia}}$. Here, the last term is the conventional diamagnetic susceptibility of a superconductor.

To estimate the first term χ_{para} , we use the methods of invariants and note that for a cubically symmetric crystal, all thermodynamic and response functions should depend on the symmetry invariance of the cubic group O_h , which are in lowest quadratic approximation corresponding to the spherical group $O(3)$. As such, the susceptibility χ_{para} should be a function of the magnetic moments of the Cooper pairs which contribute to the symmetry invariants. There are in general three symmetry invariants here. The first one is just $\mathbf{\Delta} \cdot \mathbf{\Delta}$, the second one is $\mathbf{\Delta} \cdot \mathbf{B}$. The additional anisotropy axis, e.g. orbital ordering or background nematicity associated with some vector \mathbf{b} results in another invariant as $\mathbf{\Delta} \cdot \mathbf{b}$. In the vicinity of the phase transition, we can use the Taylor expansion to obtain:

$$\chi_{\text{para}}(\mathbf{\Delta} \cdot \mathbf{b}, \mathbf{\Delta} \cdot \mathbf{B}) = \chi_{\text{para}}(0, 0) + \chi'_{\text{para}}(0, 0) (\mathbf{\Delta} \cdot \mathbf{b}) + \chi'_{\text{para}}(0, 0) (\mathbf{\Delta} \cdot \mathbf{B}) + (\text{high order terms}) \quad (4)$$

Here we assume that $(\mathbf{\Delta} \cdot \mathbf{b})$ is positive, and in general, we take its modulus.

In using this expression, the total free energy of the superconductor in the lowest order with superconducting order parameter can be written in the form:

$$F(\mathbf{\Delta}) = \alpha (\mathbf{\Delta} \cdot \mathbf{\Delta}) + \beta (\mathbf{\Delta} \cdot \mathbf{\Delta})^2 + \mathbf{M} \cdot \mathbf{B} \quad (5)$$

where the magnetization of the superconductor is equal to $\mathbf{M} = \chi_{\text{super}} \mathbf{B}$. After the substitution of the expressions for the appropriate susceptibilities, we obtain the final expression for the free energy

$$F(\mathbf{\Delta}) = \alpha (\mathbf{\Delta} \cdot \mathbf{\Delta}) + 2\delta (\mathbf{\Delta} \cdot \mathbf{b}) (\mathbf{B} \cdot \mathbf{B}) + \mu (\mathbf{B} \cdot \mathbf{B}) + (\text{high order terms}) \quad (6)$$

Minimization of this expression with respect to the vector order parameter, $\mathbf{\Delta}$, after some algebraic manipulations, gives the following equation for the superconducting energy gap $\Delta = (\mathbf{\Delta} \cdot \mathbf{\Delta})^{1/2}$:

$$\alpha \Delta + 2 \beta \Delta^3 = \pm \delta b B^2 \quad (7)$$

here b is the modulus of the vector \mathbf{b} . Introducing the notation for the gap in the zero magnetic field as $\Delta(B=0) = \Delta(0) = \Delta_0 = (-\alpha/2\beta)^{1/2}$ we can finally obtain

$$\Delta(B) = \Delta_0 - \delta b B^2 / 2 |\alpha| \quad (8)$$

Here α , β , δ are the parameters of the Ginzburg-Landau expansion. Thus, the gap value has a quadratic dependence on magnetic field. Note that as usual $\alpha = a(T - T_c)$ and β , δ are temperature independent constants. The superconductivity in the proposed orbital ordered state is expected to have a vector order parameter, describing an effective spin of Cooper pairs. This vector order

parameter is associated with the three-fold degeneracy of the t_{2g} bands of $3d$ electrons. The specific form of the order parameter depends on the details of the pairing mechanism. However in general, in systems with degenerate bands, nontrivial spin pairing may arise which is associated with an isotropic s-type gap.

We also checked the tunneling spectra of junctions with $(\text{Nd, Ce})_2\text{CuO}_4$ (NCCO) and $(\text{Pr, La, Ce})_2\text{CuO}_4$ (PLCCO) systems and discovered that they also exhibit the $\Delta \sim -B^2$ relation, as shown in Supplementary Figure 4. Naturally, cuprates and LTO are very different from each other in many ways, and yet, they both exhibit the same behavior. This indicates that perhaps occurrence of symmetry breaking leading to the vector order parameter is a rather common phenomenon, and this can be used to probe signs of symmetry breaking induced by orbital (and other types of) ordering.

Supplementary Note 5

Magnetoresistivity and the upper critical field

Magnetoresistivity (MR) in LTO changes from positive to negative as temperature is increased. The negative MR is nearly isotropic, whereas the positive MR shows clear anisotropy (see Figure 3b in the main text and Supplementary Figure 5). The observed MR is positive above superconducting transition temperature in the proposed orbital ordered (OO) nematic state, and negative above the orbital ordering transition. In the (OO) nematic phase, the coherence of the Landau quasi-particles is significantly improved, and the Fermi-liquid approach may be applicable as in normal metals. But in ordinary metals, the application of a magnetic field parallel to the thin film does not usually lead to any dramatic changes in the transport properties. However, for a 2D electron gas in the strongly correlated Fermi liquid regime, the positive magnetoresistance comes about due to electron-electron interactions^{10,11} and has the following form:

$$\text{DR}(B, T) \propto \left(\frac{B}{T}\right)^2 \quad (9)$$

In both cases, when it is perpendicular to the applied current I and when it is parallel to the applied current I , the magnetic field has small effect on the orbital motion of the electrons (unless the field is very strong).

When the OO nematic state is destroyed at $T > 40$ K, there may still be some “fluctuating” islands. We call them “fluctuating” because they may be not stable and have some finite life time, but they serve as additional (magnetic) scattering centers for the electron transport. When the magnetic field is applied, some of these islands dissolve away and the resistivity decreases. Indeed, this is similar to the negative magnetoresistance phenomena observed by Bergman when he covered thin metallic Mg films with small controlled quantities of a magnetic ion like Fe, or a heavy ion with large spin-orbit coupling like Au (ref. 12). With the increase of the density of the spin-orbit scattering centres, he observed dramatic changes in the size and sign of

magnetoresistance as a function of field: the magnetoresistance changed from negative to positive with increasing number of spin-orbit scattering centers. This is very similar to what we observe in LTO.

From the temperature dependence of resistivity in fields, we extracted the upper critical field. As shown in Supplementary Fig. 6, the B_{c2} at 90% and 50% of normal state resistivity (R_n) can be fitted by $B_{c2}(T) = B_{c2}(0)[1 - (T/T_c)^2]/[1 + (T/T_c)^2]$ derived from the Ginzburg-Landau theory. Extrapolating to the zero temperature limit, we get B_{c2} to be between 18 and 22 Tesla.

Supplementary Note 6

Structure characterizations

The LiTi_2O_4 has a cubic symmetry ($Fd3m$). The lithium cations, Li^+ are located at the tetrahedral $8a$ sites. The titanium cations, Ti^{3+} and Ti^{4+} are occupying the octahedral $16d$ sites. Our LTO thin films grown on (001)- MgAl_2O_4 (MAO) substrates show pure (001) peaks, indicating c -axis orientation. The φ -scan using the (404) reflection confirms that LTO films are epitaxially grown (Supplementary Figure 7). Temperature dependence of an X-ray diffraction peak reveals a smooth thermal expansion as shown in Supplementary Figure 8.

Supplementary References

1. Shan L. *et al.* Distinction between the normal-state gap and superconducting gap of electron-doped cuprates. *Phys. Rev. B* **78**, 014505 (2008).
2. Smith, C. W. & Dolan, P. J. Determining transport parameters for superconductor/normal metal point contacts at fixed temperature from conductance versus magnetic field data. *Physica C* **471**, 285-289 (2011).
3. Daghero, D. & Gonnelli, R. S. Probing multiband superconductivity by point-contact spectroscopy. *Supercond. Sci. & Tech.* **23**, 043001 (2010).
4. Blonder, G. E., Tinkham, M. & Klapwijk, T. M. Transition from metallic to tunneling regimes in superconducting microconstrictions: Excess current, charge imbalance, and supercurrent conversion. *Phys. Rev. B* **25**, 4515-4532 (1982).
5. Krasnov, V. M., Kovalev, A. E., Yurgens, A. & Winkler, D. Magnetic field dependence of the superconducting gap and the pseudogap in Bi2212 and $\text{HgBr}_2\text{-Bi2212}$, studied by intrinsic tunneling spectroscopy. *Phys. Rev. Lett.* **86**, 2657-2660 (2001).
6. Ning, Y. X. *et al.* Observation of surface superconductivity and direct vortex imaging of a Pb thin island with a scanning tunneling microscope. *Europhys. Lett.* **85**, 27004 (2009).
7. Eskildsen, M. R. *et al.* Scanning tunneling spectroscopy on single crystal MgB_2 . *Physica C* **385**, 169 (2003).
8. Mukhopadhyay, S., Sheet, G., Raychaudhuri, P., & Takeya, H. Magnetic-field dependence of superconducting energy gaps in $\text{YNi}_2\text{B}_2\text{C}$: Evidence of multiband superconductivity. *Phys. Rev. B* **72**, 014545 (2005).
9. Hanaguri, T. *et al.* Coherence factors in a high- T_c cuprate probed by quasi-particle scattering off vortices. *Science* **323**, 923-926 (2009).

10. Lee, P. A. & Ramakrishnan, T. V. Magnetoresistance of weakly disordered electrons, *Phys. Rev. B* **26**, 4009-4012 (1982).
11. Lee, P. A. & Ramakrishnan, T. V. Disordered electronic systems, *Rev. Mod. Phys.* **57**, 287-337 (1985).
12. Bergman, G. Measurement of the magnetic scattering time by weak localization. *Phys. Rev. Lett.* **49**, 162-164 (1982).
13. Johnston, D. C., Swenson, C. A. & Kondo, S. Specific heat (1.2–108 K) and thermal expansion (4.4–297 K) measurements of the 3d heavy-fermion compound LiV_2O_4 . *Phys. Rev. B* **59**, 2627-2641 (1999).
14. Geng, H. X. *et al.* Investigations on preparation, upper critical field and low temperature thermal expansion of LiTi_2O_4 superconductor. *Physica C* **432**, 53-58 (2005).